



Effect of salinity and water depth on the performance of doubly inclined solar still

Ganesh Bapu Shirsath^a, Raj Ganesh S. Pala^{b,*}, K. Muralidhar^a, Sameer Khandekar^a

^aDepartment of Mechanical Engineering, Indian Institute of Technology Kanpur, Kanpur 208016, UP India, Tel. +91-5122597429, email: shirgan@iitk.ac.in (G.B. Shirsath), Tel. +91-5122597182, email: kmurli@iitk.ac.in (K. Muralidhar), Tel. +91-5122597038, email: samkhan@iitk.ac.in (S. Khandekar)

^bDepartment of Chemical Engineering and the Material Science Programme, Indian Institute of Technology Kanpur, Kanpur 208016, UP India, Tel. +91-5122596143, email: rpala@iitk.ac.in (R.G.S. Pala)

Received 15 October 2017; Accepted 1 July 2018

ABSTRACT

Performance of a doubly inclined solar still carrying pure water, salt water and seawater is explored experimentally and via mathematical models. Quantities of interest are the amount of water produced and temperature distribution within the solar still. The match between the model and experiments is qualitatively good, except that the model temperatures turn out to be higher, leading to an increase in the theoretical water production. The presence of solutes is seen to diminish water productivity, and the reduction in vapor pressure with solute concentration is the factor most responsible for this trend. The effect of cycle time and condensing film thickness on water production in context with the hydrophobic and hydrophilic glass surface has also been examined within the framework of the mathematical model. The extreme sensitivity of water production to water depth for small depths is explained in terms of the large latent heat of evaporation. Since lowering the water depth increases water production, this possibility of compensating for reduction in vapor pressure with salt concentration is explored. Large water production rate in a basic solar still is possible with a proper choice of operating parameters.

Keywords: Solar still; Water production; Modeling; Fresh, salt and seawater; Vapor pressure

1. Introduction

Solar still is a device wherein contaminated water in a basin is evaporated using solar energy and the water vapor is condensed on a suitably located cooler glass surface and collected from this surface. The motivation behind the process is to distil impure water at an affordable cost. The performance of the solar still depends on various design parameters [1], mainly water depth and air gap, glass absorptivity and thickness and the extent of water contamination, apart from solar flux and ambient temperature [2,3]. Despite low cost, the solar still is constrained by a limited water production rate that has

hampered wide-spread adoption of the process as a viable source of clean water.

Experiments reported in the literature show controlling factors in a solar still to be the initial water quality [4], depth of water inside the solar still [5–7], thickness of glass cover [8,9], glass cover inclination [7,10], insulation thickness [11], air velocity [12], cavity geometry [13] and the air gap between water and the glass cover [14]. Rubio et al. [13] developed a model for estimating the mass flux based on the difference in the water and cover temperatures. Water production was found to be independent of cavity geometry for small-sized equipment for given water and cover temperatures. Madhlopa [15] developed two models involving radiative heat transfer with and without view factor. Radiative heat transfer was seen to be smaller with the inclusion

*Corresponding author.

of a view factor. Rahbar et al. [16] carried out numerical simulation for a single slope solar still with CFD, comparing it with a lumped model based on the Chilton-Colburn correlation, and found a close agreement. A single slope solar still was found to be superior to the double slope solar still within a given season, though not over a year. The productivity of a simple solar still increased when the water depth was reduced. Ahsan et al. [4] conducted experiments on a triangular solar still to investigate the effect of water depth on its performance. The authors found that the daily water productivity is inversely proportional to the initial water depth. Bakari et al. [8] studied the performance of a solar still with glass sheet thickness as a parameter. The smallest possible thickness was found to yield the highest water production rate. Khalifa [10] reported the overall performance of a solar still based on the tilt angle and concluded that the optimum tilt angle should be equivalent to the latitude of the location. Khalifa and Hamood [11] studied the effect of insulation thickness on the productivity of a solar still. Tellez et al. [12] investigated the effect of air velocity on the solar still and found that, above 5.5 m/s, the performance diminished. Xiong et al. [17] conducted experiments on an enhanced solar still with the use of a heat pipe and an improved condensing surface. The authors developed a numerical model for predicting the performance of the enhanced solar still using the Dunkel model. Tiwari et al. [18] developed a numerical model that included the inner and outer glass temperatures. The inner glass temperatures were seen to be in closer agreement with experiments as compared to the outer. Panchal et al. conducted the trials on indoor as well as outdoor solar still and found that the water temperature and inner glass temperature are more or less similar and in good agreement with each other [19].

Researchers have adopted various techniques to improve the performance of a solar still [20]. Mahdi et al. [21] conducted an experiment on a wick type solar still with varying percentages of NaCl inside the solar still. The authors reported two parameters, namely, lower vapor pressure and higher surface tension that affected the still performance. With increase in salinity, the performance of the solar still reduces since vapor pressure decreases, thus resulting in lower evaporation rates [22]. Higher surface tension also contributes to lower productivity of the solar still [23]. Mahdi et al. [21] found the solar still efficiency to reduce from 38% to 20% with an increase in salt concentration from 0 to 10%. Rai et al. [21,23] reported that with increase of salinity from 7% to 12% there is significant reduction in distillate collected, falling from 1.1 to 0.5 kg per unit area, respectively.

The central theme of research reported here is to provide a comprehensive understanding of the performance of a solar still. The device studied is free of enhancement features. In this respect, the productivity of the system is a lower limit of what can be obtained. Active enhancement features will increase water productivity, but at a cost. Hence, there continues to be an interest in such baseline devices. Follow-up studies will include condensation over physically textured surfaces and the careful use of membranes on the hot water side. The present study is the first in a sequence where the possibility of enhancement in water production from a passive solar still is examined. The main focus and novelty of the present study is summarized below.

Important trends in solar still performance are examined by comparing experiments with the mathematical model at continuous time points. Creation of an extensive experimental database generated over a two-year period is one of the highlights of the study. It is conclusively established that differences in vapor pressure discriminate water production with salt/seawater as against fresh water. The mathematical model rationalizes why increase in density and specific heat, and reduction in latent heat with salt concentration impact transient behavior of salt/seawater stills, as recorded in experiments. Among these parameters, sensitivity analysis shows that changes in latent heat have the greatest influence on the thermal transients. The significance of water layer height on the production of fresh water is interpreted on a day-long basis. It is shown that there is a delay in the heating rate of the water body that diminishes water production. It is not sufficiently compensated by a delay in the cooling rate, particularly after sunset. Such an analysis helps in evaluating the use of a phase-change medium in conjunction with the solar still.

Dropwise condensation patterns are recorded over the glass cover with fresh, salt and seawater. The reduction in the largest drop size with increase in salt concentration is clearly shown. The possible gains with employing a hydrophobic surface for condensations are also discussed. The possibility of including dropwise condensation within the mathematical model is examined. Passive solar stills are most likely to be used with water of very low quality and a high concentration of dissolved impurities. It is shown that water quality produced from sea/salt water stills are closely comparable to water produced from a fresh water still. Previous literature has stated a lowering of evaporation rates in water with dissolved salts with respect to fresh water. In this respect, Raoult's law is explicitly included in the model and its predictions are compared with experiments. The match is seen to be good. Dropwise, as well filmwise condensation patterns become unstable and drain off the glass cover. The procedure to be adopted for including water film thickness over the glass sheet and the cyclic process of film/drop drainage are discussed.

1.1. Apparatus

Three solar stills have been fabricated from GI sheets with a purpose of comparing their performance under identical conditions. Experiments have been carried out with pure, salt, and seawater. The stills have equal dimensions and identical materials, the base being 0.6 m × 0.6 m.

The dimensions of the solar still adopted in the present work match well with those reported in the literature for testing on a laboratory scale. The condensed water output of the solar still developed in the present work ranges from 1 to 4 L/m²-d, and is comparable to prototypes reported by other authors. Hence, it is expected that the observations of the present study will be useful in field-scale applications. Edeoja et al. [24] experimented with solar stills of dimensions 0.6 m × 0.4 m (70 mm water depth) that produced only an output of 62.9 cm³ of water per day. Anjaneyulu et al. [25] fabricated a simple solar still with dimensions of 0.875 m × 0.566 m (50 mm water depth) and collected 4 L/m²-d. Arunkumar et al. [26] constructed a double basin solar still, 0.59 m × 0.44 m (440 mm overall height), with water produc-

tion up to 2.9 L/m²-d. The comparison can also be stated in terms of the still effectiveness. It is an energetic measure and is calculated as water yield per m²/s multiplied by the latent heat of vaporization of water, normalized by the average solar flux. Table 1 compares effectiveness of solar stills reported in the literature. The solar still under discussion is seen to be acceptable in terms of its performance.

In the present study, the tilt angle of the glass surface of the solar still is maintained at 28°, being equal to the latitude of the city of Kanpur (India), where experiments were carried out. The double inclination, as shown in Fig. 1, keeps the incident solar radiation at near normal incidence over a given day. Double inclination has a second advantage in terms of water collection since the condensate drained from the entire surface reaches a common point, thus raising the collection efficiency. Acrylic channels on the sides of the solar still have been used to collect the condensate. These channels emerge from the still at a given point where water is collected in a measuring beaker. Density measurement and chemical analysis of the condensate is, however, based on samples collected at the glass sheet itself. The base of the solar still is blackened on a weekly basis to improve

absorption of solar energy and is thermally insulated. Glass is fitted on the top of the solar still with putty to prevent leakage of water vapor.

1.2. Measurement procedure

Each of the three solar stills is instrumented with the six K-type thermocouples at distinct locations in the vertical direction (Fig. 1).

Thermocouples are connected to a computer via a 24-channel National Instruments (NI) temperature measurement card that enables data logging through a PC over a period of several days. Thermocouples are individually calibrated against a standard and are periodically interchanged to examine and ensure repeatability. Temperatures are recorded above and below the glass surface, in water, and at the base using the data logger. The distillate is also collected on an hourly basis. The wind velocity outside the solar still is periodically measured with the use of a pitot static tube and an inclined-tube manometer. Solar flux is measured in a clear area with the use of an Acksen-PV3 solar data logger and software (Electrosoft) to store the read-

Table 1
Comparison of effectiveness of solar stills reported in the literature

	Present experiment	Dev et al. [5]	Kumar et al. [27]	Elango et al. [28]	Omara et al. [29]	Sathyamurthy et al. [30]
Yield (kg/m ²)	3.09	4.15	3.9	3.56	3.575	4.7
Average solar flux (W/m ²)	229.33	307.5	173.33	322.97	318.96	256.72
Effectiveness	0.34	0.34	0.58	0.28	0.28	0.47

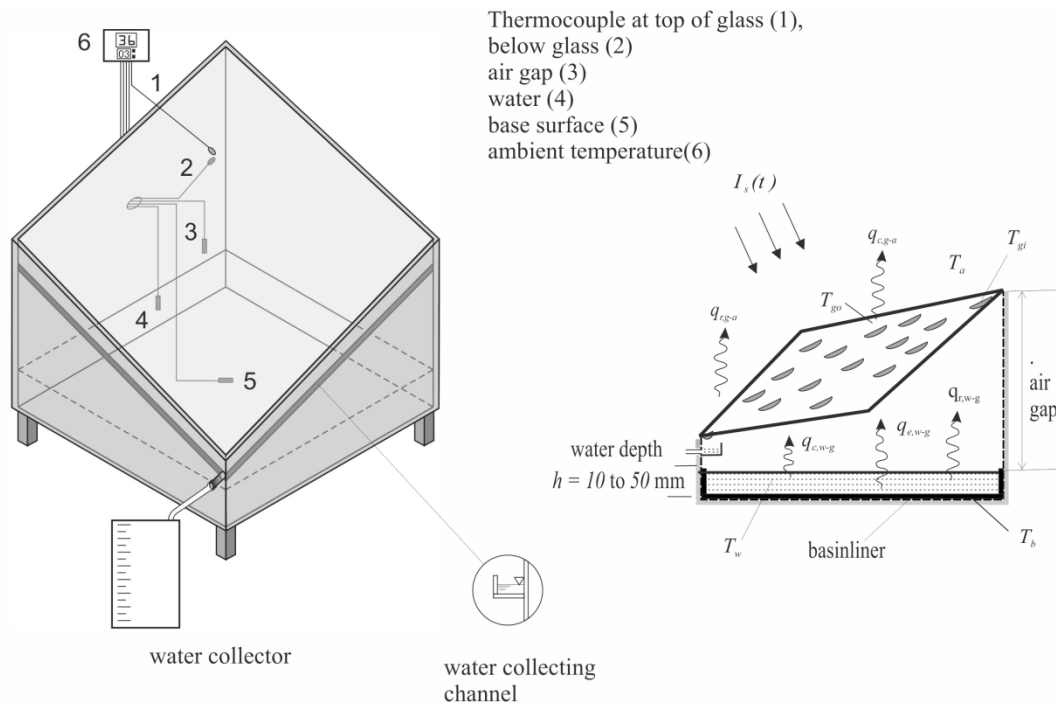


Fig. 1. (left) Schematic diagram of a doubly inclined solar still; numbers indicate thermocouple positions and (right) cross-sectional view of the solar still.

ings within a clear area. Density of water is measured with the help of a precision weighing balance and a calibrated beaker of 40 ml capacity. Solar still experiments have been carried out on the terrace of a three-floor building, clear of trees and adjacent structures. Since the water production rates of the present study are close to those in the literature, the performance of the solar still fabricated may be taken as satisfactory. Explicit validation against a mathematical model is discussed in the following section. Experiments were carried out over a period of 8–10 weeks though data for five consecutive days is reported. The excellent repeatability in temperature and water production data over this duration shows the measurements to be within acceptable levels of scatter.

The three solar stills individually contain salt, sea and pure water, the last being collected from a distillation system. Salt water is prepared with the addition of 25 g/L of chemically pure common salt (NaCl). Chemical composition of seawater follows the ASTM standard D1141; 98 (2013) [22]. The composition contains the following salts in grams per litre: NaCl - 24.53, MgCl₂ - 5.20, Na₂SO₄ - 4.09, CaCl₂ - 1.16, KCl - 0.695, NaHCO₃ - 0.201, KBr - 0.101, H₃BO₃ - 0.027, SrCl₂ - 0.025, NaF - 0.003, Ba(NO₃)₂ - 0.0000994, Mn(NO₂)₂ - 0.0000340, Cu(NO₃)₂ - 0.0000308, Zn(NO₃)₂ - 0.0000096, Pb(NO₃)₂ - 0.0000066, AgNO₃ - 0.00000049. Water levels were maintained constant during the experiment by adding small quantities of warm water/solution as appropriate.

2. Mathematical model

Following the literature [16,31–34], lumped analysis of a solar still is carried out as follows. From the first law of thermodynamics, energy balance equation for the water mass is given as:

$$(MC)_w \frac{dT_w}{dt} = [\alpha_w(1 - \alpha_g)I + q_w] - [q_{r,w-g} + q_{c,w-g} + q_{e,w-g}] \quad (1)$$

Symbols appearing in the model equations are defined in the section on nomenclature. Heat fluxes appearing in Eq. (1) are given by the following expression in terms of a heat transfer coefficient and the relevant temperature difference.

Convective heat transfer from the basin liner to the water body is [2].

$$q_w = h_w(T_b - T_w) \quad (2)$$

Assuming the buoyancy driven convection in water, the heat transfer coefficient (units of W/m²-K) between basin and water surface is taken as [20].

$$h_w = \frac{K_w}{X_w} C(GrPr)^n \quad (3)$$

The parameters appearing in the above correlation are given in Table 2, and to calculate the Grashof number and Prandtl number, thermophysical properties of water are used.

Radiative heat transfer from the water surface to the glass cover is [35].

Table 2

Parameter specification for the mathematical model

α_b	0.56	C_w	4190 J/kg-K
α_g	0.047	C_{w_salt}	4027.8 J/kg-K
α_w	0.2	C_{w_sea}	3978.6 J/kg-K
e_w	0.1	h_{fg}	2.345×10^6 J/kg
e_g	0.047	h_{fg_salt}	2.350×10^6 J/kg
K_g	1.05 W/m-K	h_{fg_sea}	2.356×10^6 J/kg
K_w	0.58 W/m-K	K_a	0.0285 W/m-K
X_w	0.6 m	X_a	0.6 m
C	0.54	N	1/4
L_g	5 mm		

$$q_{r,w-g} = h_{r,w-g}(T_w - T_{gi}) \quad (4)$$

With temperatures expressed in Kelvin, the radiative heat transfer coefficient (W/m²-K) between the surface of water and the glass cover is [31].

$$h_{r,w-g} = \epsilon_{eff} \rho \frac{(T_w)^2 + (T_{gi})^2}{T_w + T_{gi}} \quad (5)$$

Convective heat transfer from the water surface to glass cover is

$$q_{c,w-g} = h_{c,w-g}(T_w - T_{gi}) \quad (6)$$

Here the convective heat transfer coefficient between water surface and glass cover is [30].

$$h_{c,w-g} = 0.884 \left[(T_w - T_{gi}) + \frac{(P_w - P_{gi})T_w}{268.9 \times 10^3 - P_w} \right]^{1/3} \quad (7)$$

Evaporative heat transfer from the water surface to the glass cover is

$$q_{e,w-g} = h_{e,w-g}(T_w - T_{gi}) \quad (8)$$

The evaporative heat transfer coefficient (W/m²-K) between the water surface and glass cover is [31].

$$h_{e,w-g} = 16.273 \times 10^{-3} \times h_{c,w-g} \left[\frac{(P_w - P_{gi})}{(T_w - T_{gi})} \right] \quad (9)$$

Partial pressure of water (Pa) required in the expressions for the heat transfer coefficients can be calculated from the Antoine equation derived from the Clausius-Clapeyron equation as [31]:

$$P_w = \exp \left[25.317 - \left[\frac{5144}{T_w} \right] \right] \quad (10)$$

Here, temperature T_w is in units of Kelvin. Using the Raoult's law, vapor pressure of the salt solution can be calculated as follows.

$$\text{Salt water: } P_w = 0.9068 \times \exp \left[25.317 - \left[\frac{5144}{T_w} \right] \right] N / m^2 \quad (11)$$

$$\text{Seawater: } P_w = 0.8445 \times \exp \left[25.317 - \left[\frac{5144}{T_w} \right] \right] N / m^2 \quad (12)$$

Partial vapor pressure at the inner surface of glass is

$$P_{gi} = \exp \left[25.317 - \left[\frac{5144}{T_{gi}} \right] \right] \quad (13)$$

Heat flux through the outer glass cover is balanced by convective and radiative heat transfer to the ambient and is written as [35].

$$\frac{K_g}{L_g} (T_{gi} - T_{go}) = h_{i,g-a} (T_{go} - T_a) \quad (14)$$

The total heat transfer coefficient from glass to the ambient is the sum of the radiative and convective components [30].

$$h_{i,g-a} = h_{r,g-a} + h_{c,g-a} \quad W / m^2 - K \quad (15)$$

With temperatures in Kelvin, the radiative heat transfer coefficient is given as [31].

$$h_{r,g-a} = \epsilon_g \sigma \left[\frac{(T_{go})^4 - (T_{sky})^4}{T_{go} - T_a} \right] \quad (16)$$

The convective heat transfer coefficient (W/m^2-K) for the outer surface of glass is related to air velocity (in m/s) and is given as [20].

$$h_{c,g-a} = 2.8 + (3.0 \times v) \quad (17)$$

Energy balance equation applied to the glass cover is obtained as

$$\alpha_g I + (q_{r,w-g} + q_{c,w-g} + q_{e,w-g}) = \frac{K_g}{L_g} (T_{gi} - T_{go}) \quad (18)$$

The blackened base liner of the solar still is heated by the incident solar flux while being cooled by the water body next to it, losses to the environment through the support below, and direct radiation to the environment. Hence, the energy balance equation applicable for the base liner is written as [20].

$$\alpha_b (1 - \alpha_g) (1 - \alpha_w) I = (q_w + q_b) \quad (19)$$

Heat transfer from basin liner to the atmosphere is [16]

$$q_b = h_b (T_b - T_a) \quad (20)$$

The heat transfer coefficient is obtained from the natural convection correlation [35].

$$h_b = \frac{K_a}{X_a} 0.27 \times (Ra)^{\frac{1}{4}} \quad (21)$$

The heat capacity of the glass cover can be included in the present mathematical model. It will appear in the transient term for variation of glass temperature in the glass

cover energy balance equation. Since the glass temperature difference is small, its effect is negligible and hence the transient term including glass cover heat capacity can be dropped from analysis. The detailed analysis of the effect of heat capacity of glass and basin has also been reported in a recent study (Sivakumar and Ganapathy Sundaram, [36]). The authors show that inclusion of these terms increases the daily cumulative water yield just marginally ($\sim 0.129 \text{ kg}/m^2$) and is hence not significant.

Parameters appearing in the above set of equations are summarized in Table 2. The mathematical model comprises solving the first order nonlinear differential equation for water temperature [Eq. (1)] subjected to a specified initial condition and time-dependent solar fluxes, air velocity, and ambient temperature as appropriate to the location of interest. The differential equation of the model has been solved using a 4th order Runge-Kutta scheme, starting from cold conditions of the solar still. The code was run for a period of ten days of solar heating before comparison with the experimental data. The hourly yield of water (kg/h) from the solar still is calculated as [20].

$$M_{ew} = \frac{h_{e,w-g} (T_w - T_{gi})}{h_{fg}} \times 3600 \times A_s \quad (22)$$

Since the glass temperature is sufficiently cooler than vapor, one can assume the entire vapor to condense over the glass sheet with δ^n as the instantaneous film thickness at a time instant n , the growth rate of film thickness in discretized form is expressed as follows:

$$\frac{\delta^{n+1} - \delta^n}{\Delta t} = \frac{M_{ew}^n + M_{ew}^{n+1}}{2} \left(\frac{1}{\rho_v A_{g, \text{glass}}} \right) \quad (23)$$

Eq. (23) is integrated over several days during which the film repeatedly forms and is drained away. On a hydrophobic surface, condensation is in the form of drops and the cycle time is expected to be smaller. The presence of a film of water on a glass surface is accounted for in the model by altering the effective thermal conductivity and effective absorptivity of the glass surface and correcting for slight change in the air gap thickness.

3. Results and discussion

While enhancement features have been reported to increase water productivity, the basic solar still continues to be of interest, owing to its simplicity, robustness and cost-effective features. The doubly-inclined solar still considered in the present work is expected to have an advantage on a year-round basis. In the present experiments, quantities measured include temperatures at distinct locations within the still and the hourly water production rate. These are compared against the predictions of a mathematical model. Experiments have been carried out on clear as well as partly cloudy days with three identical solar stills containing fresh water, salt water and seawater, respectively. The simulation employs solar fluxes, ambient temperature, and air velocity that have been measured over a period of five consecutive days. The contrasting roles played by water depth in water production as compared to the air gap are investigated. A sensitivity analysis of thermophysical properties of fresh, salt and sea-

water has been carried out to rationalize factors leading to reduction in water production. The mathematical model is extended to include a condensate water layer whose thickness increases with time till a critical state is reached and the film is drained away. Instantaneous condensation patterns formed on the glass surface in each of the salt, sea and fresh water are recorded and subsequently analyzed. The density of the condensate at the glass surface is recorded to ascertain that the distillation process is effective. In addition, the condensate has been subjected to full chemical analysis using an inductively coupled plasma mass spectrometry technique. In this respect, the reported study comprehensively establishes the performance of a basic solar still.

3.1. Comparison of clear and cloudy days

Fig. 2 compares sequences of clear and cloudy days in terms of environmental parameters that affect the solar still. These include solar flux (top row), ambient temperature (middle) and air velocity (bottom). On a cloudy day, the solar flux is interrupted and this in turn, alters the ambient temperature. On clear days, the flux variation along with ambient temperature shows a regular trend, with a maximum achieved at around noon. Air velocity does not show a definite trend and is not correlated with the solar flux.

Fig. 3 presents the cumulative water production data (units of kg/m²) when pure water is used. The top row is experimentally derived for clear as well as cloudy days. The maximum water production is found to be 2.9 kg/m² on a clear day and is expectedly smaller on cloudy days. Model prediction under identical flux, ambient temperature, and air velocity conditions are shown in the middle row. A reasonable match is seen between the two

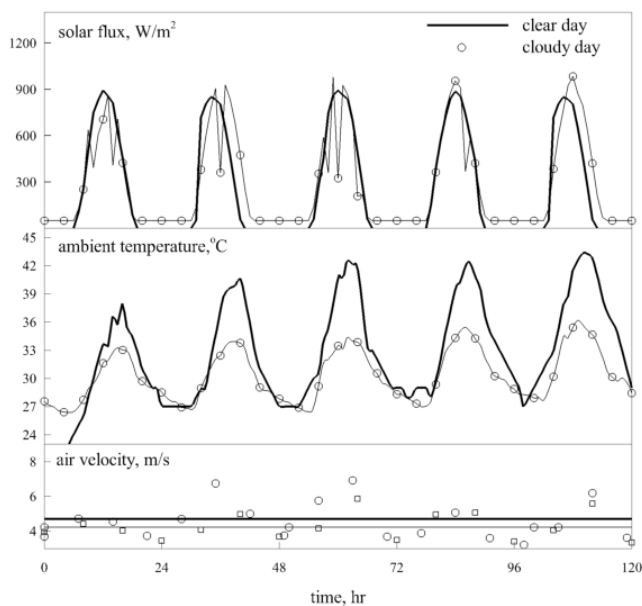


Fig. 2. Variation of solar flux, ambient temperature, and air velocity on clear (thick line) and cloudy (thin line) days over a period of five consecutive days. Straight lines for air velocity indicate the average recorded over a day.

sets of data, the model predictions of water production being higher on both cloudy and clear days. This trend is expected because the model does not entirely factor in heat losses from below the basin, where temperatures are the highest, to the ground and the ambient. The bottom row shows the water production rate (kg/m²-h) from the mathematical model. The experimental data are close but smaller and are not shown. Water production rate follows the trend of the solar flux on cloudy and clear days, being a maximum in the afternoon and a minimum at the start and the end of the day.

Clear periodicity in water production also shows that water in the basin cools off during the night and has to be freshly heated in the morning hours. The association between solar flux and water production continues to be close on clear and cloudy days, the cloud interruptions diminishing water production. The model succeeds in capturing the transient heating period of water before the commencement of evaporation. Evaporation fluxes scale with water temperature and are a maximum closer to the afternoon on clear days, when the solar flux is also at its peak.

3.2. Comparison of solar stills with distilled water, salt and seawater

Fig. 4 shows water production data for salt, sea and pure water solar stills for a period of five clear days. The

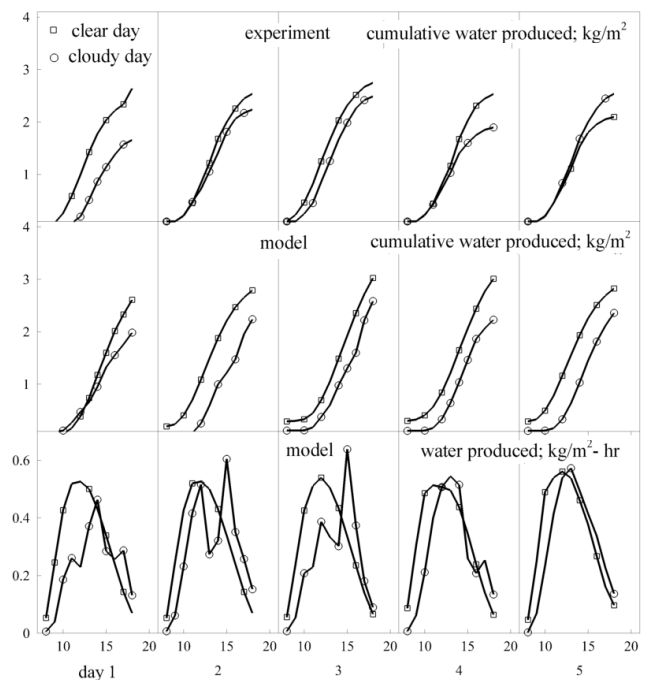


Fig. 3. Comparison of water produced from experiments with the mathematical model over five clear and cloudy days. Top row is the cumulative water produced in experiments, units of kg/m²; middle row is the cumulative water produced as determined from the model; bottom row is the water production rate from the model in units of kg/m²-h at water depth of 10 mm.

top row records the cumulative water production from experiments. The maximum water production among the five days is 2.99 kg/m² for pure water, 2.37 kg/m² for salt and 2.0 kg/m² for seawater. The production rates at any other point of time follow this order. This trend is expected because a salt solution has higher density and, for a given solar flux, heats up at a slower rate. In addition, the salt solution including seawater has a lower vapor pressure that diminishes evaporation rates. The effective salt content of seawater being higher, its productivity is further lowered relative to salt water.

The bottom row of Fig. 4 compares the cumulative water produced in units of kg/m² for pure, salt, and sea-water from the mathematical model. Here, thermophysical properties of the three fluids were suitably provided, apart from information on latent heat and vapor pressure. The model predicts a lowering of water production with increasing salt content and is in overall agreement with the experimental data.

Fig. 5 top row shows the experimentally obtained variation of water produced per hour for salt, sea and pure water solar stills. The data is in overall agreement with the bottom row, the water production rate in kg/m²-h obtained from the model. The trends observed follow the variation of solar flux with time of the day, the water production rate being consistently less for seawater relative to pure water. The instantaneous water output is closely associated with solar flux, attaining a maximum soon after mid-day. The slight delay in the occurrence of the maximum beyond noon time is related to the initial sensible heating of the water body in the still. A consequence of the correlation between water production and solar flux is that evaporation (and water production) diminishes to unacceptably small levels later in the evening. Basin losses being larger in the experiment, the cooling off phase is brought out sharply in Fig. 5. Differences among the three liquids arise primarily from thermal capacity effects.

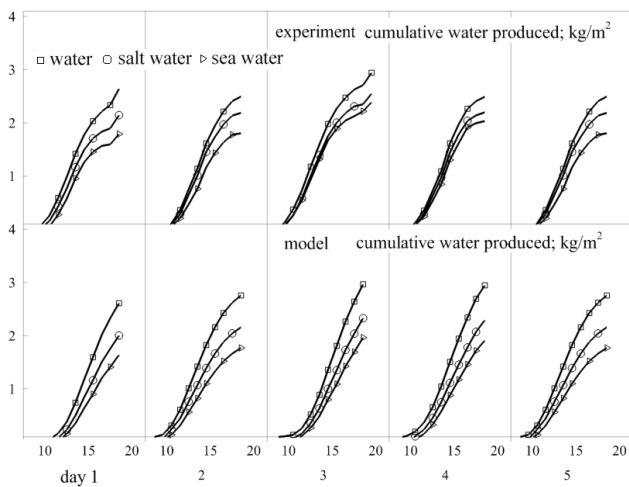


Fig. 4. Comparison of water produced from experiments against the mathematical model over five clear days for pure, salt and seawater. Top row is the cumulative water produced in experiments (kg/m²); bottom row is the cumulative water produced from the model (kg/m²) at water depth of 10 mm.

The lower vapor pressure for salt and seawater lowers evaporation rates, lowers the accompanying latent heat contribution. Numerical experiments show these to be a secondary influence. The sensitivity of water production to the thermophysical properties is discussed in Section 4.

Fig. 6 shows the variation of inner and outer glass surface temperatures obtained from experiments. The corresponding basin temperature is also shown. While sea and salt water temperatures were distinct from pure water, the

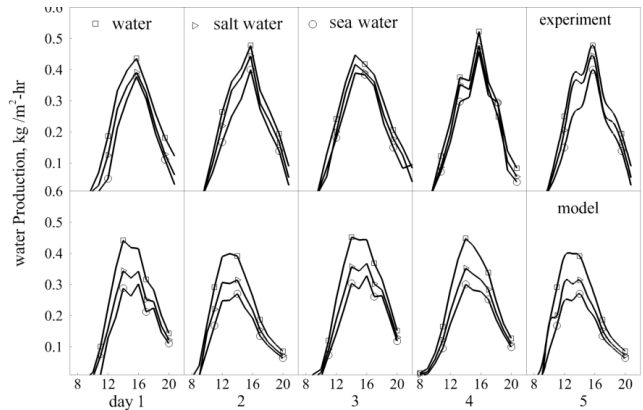


Fig. 5. Comparison of water produced from experiments against the mathematical model over five clear days for pure, salt and seawater. Top row is the water produced in experiments (kg/m²-h); bottom row is the water produced from the model (kg/m²-h) at water depth of 10 mm.

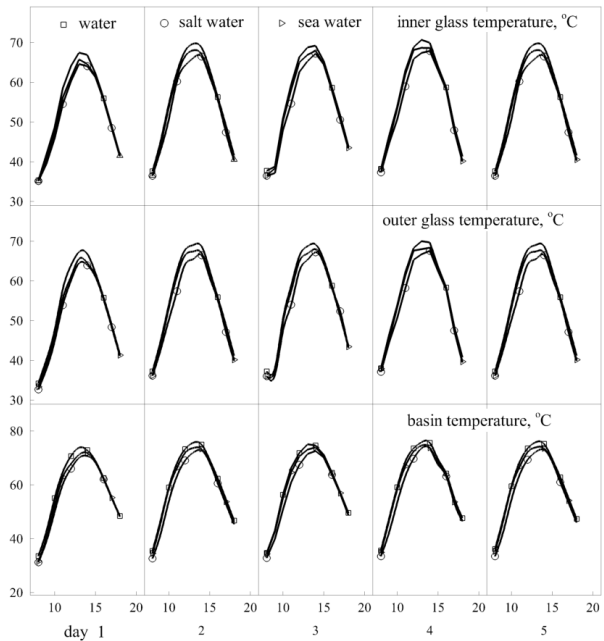


Fig. 6. Measured variation of inner glass, outer glass and basin temperatures from pure, salt and seawater solar still for a period of five clear days at a water depth of 10 mm. Glass surface temperatures are distinct among fresh, salt and seawater experiments.

corresponding differences in glass temperatures were not measurable. The glass temperatures follow the solar flux variation on a daily basis. The temperature drop across the glass sheet is around 5°C, but the exterior of the glass sheet temperature is around 20°C higher than the ambient. These temperature excesses point towards a large thermal resistance that limits condensation. Water production rates will be certainly be enhanced with a smaller glass sheet thickness and larger air velocities. High thermal resistance is also why basin temperature differences are measurable at the glass surface. Solar energy absorption by the glass surface is another reason for large glass temperatures that lowers water production.

Fig. 7 compares experimental and model water temperatures for the three fluids studied over five clear days. In experiments, the thermocouple was placed at the center of the water body. The overall trends are similar; expect that the model temperatures (bottom row) are higher. The quantitative difference arises from inexact match of model parameters such as the properties of water and wood with the experiment, losses from the basin to the ambient being an important factor. Both, model data and experimental measurements show that the increase in pure water temperature is the highest and that of seawater is the lowest, for the experimental duration considered. Since losses are under-predicted in the model, water temperature rises rapidly, diminishing the duration of the thermal transient. Hence, evaporation starts early, leading to a higher yield of water. When the solar flux starts to reduce, temperatures fall but reduced losses ensure that the cooling phase predicted by the model is also slower. As a result, water production predicted by the model remains high for a longer period (Figs. 4 and 5) and water temperature at the end of the day is also high.

The mathematical model shows appropriate sensitivity to the input solar flux, water depth, and solute concentration in fresh water. The degree of model sensitivity to the process parameters matches experimental data. An instant-to-instant agreement between the model and experiment cannot be expected. This is because the model is based on lumped analysis and ignores spatial distribution in water

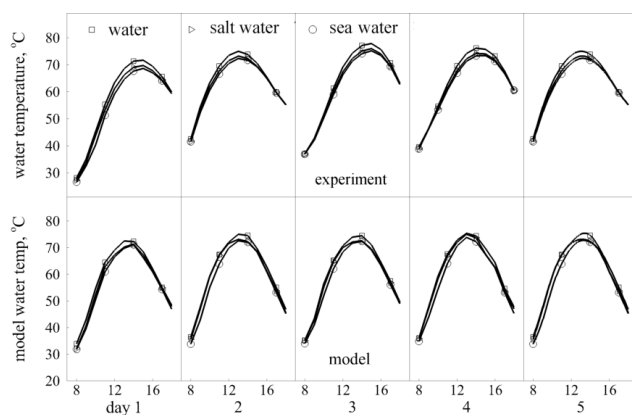


Fig. 7. Variation of water temperature from pure, salt and seawater solar stills over five clear days at water depth of 10 mm. Top row records experimental data and bottom row is from the mathematical model.

temperature. It neglects double-diffusive convection of thermal energy and moisture in air.

Fig. 8 compares the basin temperature of the solar still with the one obtained from the mathematical model. Since the basin is blackened, the basin temperature is the highest within the solar still. The ambient serves as the sink for the heat transfer process. The model temperatures (bottom row) are consistently higher than the measured (top row). The peak basin temperatures are around 10°C higher than the peak water temperature, but vary in a manner that is consistent with the solar flux. The large temperature difference between water and the base is also indicative of a large thermal resistance that limits the still performance. A smaller water mass can reduce thermal resistance and reduce the temperature drop. The effect of water depth on still performance is studied in Section 4.

A comparison of the mathematical model with measurements in Fig. 9 shows the model to capture essential aspects of the solar distillation process. Differences arise from uncertainties in the model parameters related to geometric dimensions, material properties and phenomenological correlations. To ascertain the sensitivity of model predictions, the cumulative water production was determined from the model using three different time-dependent inputs: (i) solar flux data, (ii) measured basin temperature, and (iii) measured water temperature. Fig. 9 shows this comparison in terms of the cumulative water quantity predicted by the mathematical model. The predictions with solar flux and basin temperature are practically identical, indicating a satisfactory choice of parameters in the determination of the basin temperature. The mathematical model can be simulated with the time-varying water temperature as the input. The predicted water output with this approach is lower than the other two, namely, when solar flux and basin temperature are the input parameters. It is, however, in agreement with the water output determined from the experiments. In this respect, correct simulation of the average water temperature emerges as the most important step in solar still modeling.

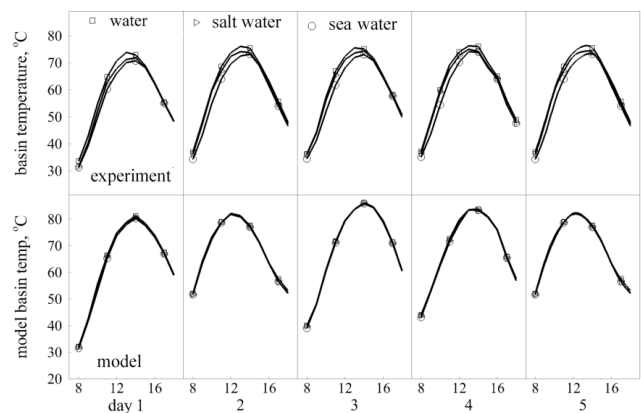


Fig. 8. Variation of basin temperature from pure, salt and seawater solar stills over five clear days at water depth of 10 mm. Top row records experimental data and bottom row is from the mathematical model.

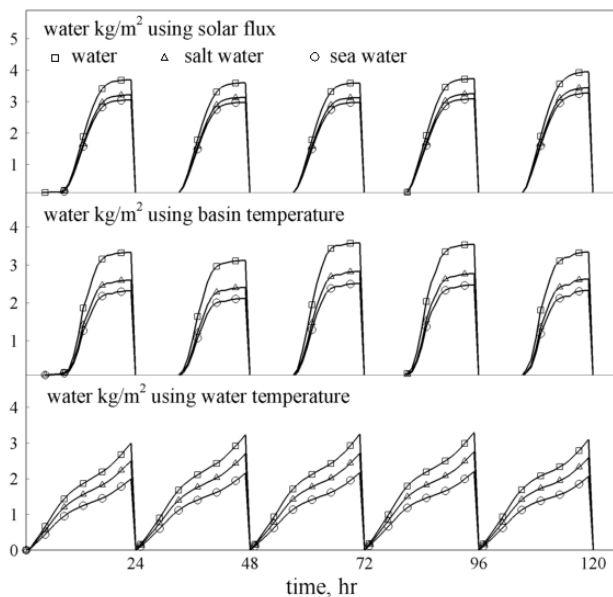


Fig. 9. Model variation of water produced from pure, salt and seawater solar stills over five clear days. Top row shows water production when the input data is the measured solar flux. Middle row uses the measured basin temperature as an input. The bottom row is a prediction of water production when the measured water temperature is provided as an input to the model.

3.3. Effect of pure water, salt water and seawater on the condensation patterns

Since the vapor leaving the solution is expected to be practically pure H_2O , the condensation patterns with fresh, salt and seawater are expected to be similar. However, differences may arise from glass surface temperature and vapor velocity. These may in turn reduce the rate of condensate formation and the water produced.

Condensation patterns were imaged with pure, salt and seawater, initially in the solar still and later from a covered beaker under laboratory conditions. Experiments were carried out with a glass surface inclined at 29° with the horizontal. For an uncoated surface, condensation was seen to form a film and the time-wise evolution of the condensation pattern could not be studied. To reveal possible changes in the condensation process with time, the glass surface $75 \times 25 \text{ mm}^2$ in area was functionalized to make it hydrophobic. Condensation patterns were recorded over $25 \times 25 \text{ mm}^2$ area using a Sony digital camera at selected time instants.

Fig. 10 compares condensation patterns recorded with fresh, salt, and seawater. At a contact angle of 54° , the initial drops coalesce to form large puddles, similar to a film. The image quality improves at a contact angle of 110° and clear drops are formed. The first drop to slide off the glass surface occurs at a time instant in the range 1220–1240 s. The condensation process with the three liquids has an observed cycle time of 6–10 s between drop instability and is related to the vapor flux. Overall, the three liquids demonstrate similar condensation dynamics at the glass sheet and do not introduce unexpected phenomena that could slow the water production step. It may also be noted that heat transfer coefficient is higher for dropwise conden-

sation as compared to the filmwise. This result can be utilized for reducing the thermal resistance at the glass cover [37]. Effect of the film thickness on water temperatures and water production can be evaluated jointly with absorptivity and thickness of glass. To investigate the equivalent film thickness arising from the dropwise condensation, drop diameters were measured from Fig. 10. Over a cycle time of 1200 s, the average drop diameter was estimated to be 1.3 mm. To simplify analysis, the dropwise condensation patterns were replaced by an equivalent uniform film of 1 mm thickness. For pure filmwise condensation, the average liquid film thickness is greater than 1 mm. The above data is combined with Eq. (23) to study its effect on temperatures in the still and water production. Absorptivity of water and glass are taken to be equal ($= 0.95$) in the discussion below.

3.4. Effect of cycle time and film thickness on water production

The nature of condensation of the vapor flux falling on the inclined glass sheet can be in the form of thin film [33–34] or a collection of drops. The former is realized when the surface is hydrophilic while distinct liquid drops form on a hydrophobic surface. The stability of liquid drops on an inclined hydrophobic surface has been discussed by Sikarwar et al. [38]. Following this study and the data of Fig. 10, dropwise condensation is modeled as a process that grows the film from zero to 1 mm in thickness at a rate determined by the water evaporation rate.

The top row of Fig. 11 shows the variation of mass flux of water depositing over the glass surface on an average clear day, a peak in the flux being visible closer to mid-day. Solving Eq. (23), the corresponding increase in the film thickness with time can be calculated and is also shown in Fig. 11. For a hydrophilic surface, water is drained away when the film thickness just exceeds 1 mm. Subsequently, a fresh film is initiated. Fig. 10 shows that a thick film is present over the hydrophilic glass surface while the average film thickness for hydrophobic surface is smaller. Frequent draining of water film over a hydrophobic surface helps keep the surface dry. Clearly a hydrophobic surface is superior to hydrophilic in this regard.

The impact of water film forming on a glass surface on the solar still properties is summarized in Table 3. As discussed in Section 2 water layer increases the conduction resistance at the glass surface, increases the energy absorbed but decreased the air gap. As discussed earlier, air gap plays a secondary role in the solar still performance. Hence, the effect of condensate layer on the glass surface is primarily to reduce the overall temperature difference available between the water body and the cooler surface, thus diminishing water production.

The effect of a condensate film on the glass sheet on the solar still performance has been determined by using the mathematical model discussed in Section 2. Glass sheet thicknesses of 1 mm and 5 mm have been considered. Condensate film thicknesses of 1 mm have also been considered. Glass and water have distinct thermophysical properties but comparable optical properties. Hence, glass and water film thicknesses can be added for the purpose of absorption calculations.

Table 3 shows no reduction in water production when the water film is included in the analysis. However, the

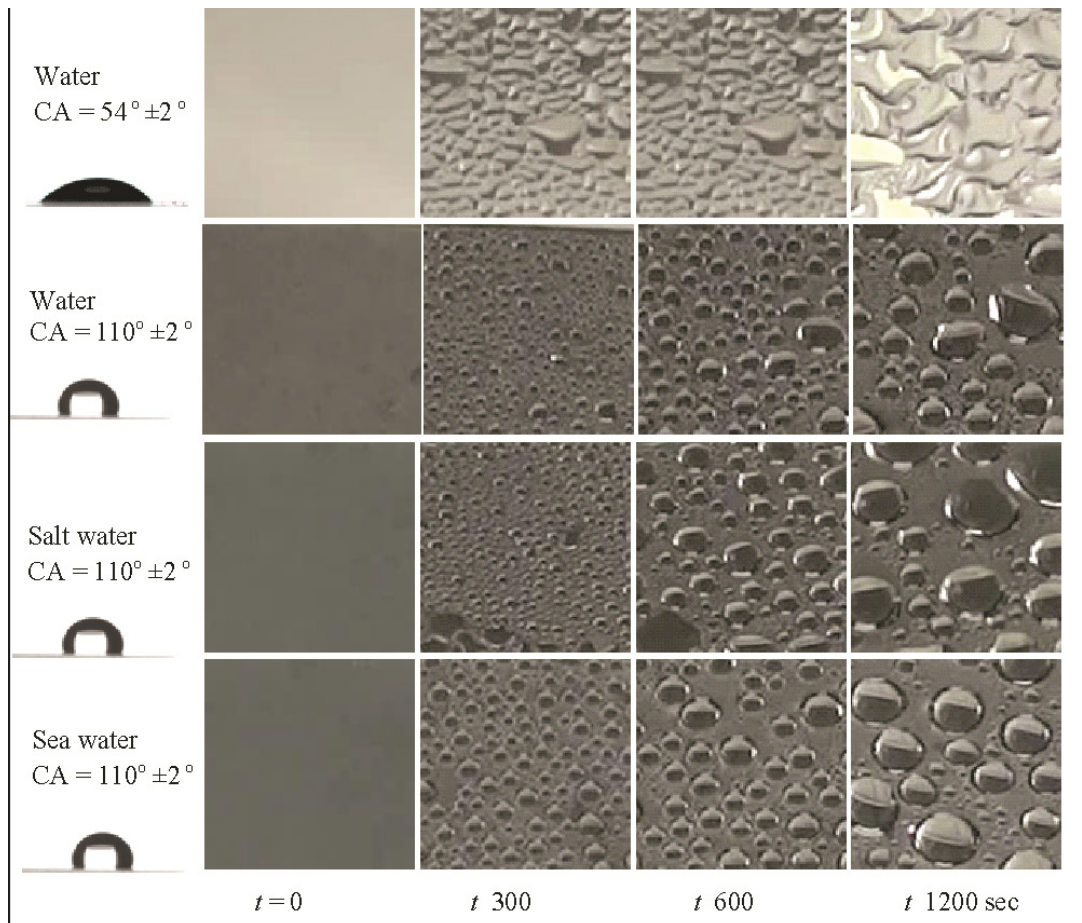


Fig. 10. Condensation patterns for water, salt and seawater formed on the underside of a chemically textured hydrophobic surface at a water depth of 15 mm, air gap 60 mm, ambient temperature 30°C and water temperature 65°C. The first column shows static drops sitting on the respective textured surfaces and the corresponding contact angle. Top row shows the filmwise condensation corresponding to hydrophilic surface with contact angle less than 90° and second row from the top shows the dropwise condensation corresponding to hydrophobic surface with contact angle greater than 90°. Third row from the top corresponds to condensation patterns for salt water and the last row is for seawater.

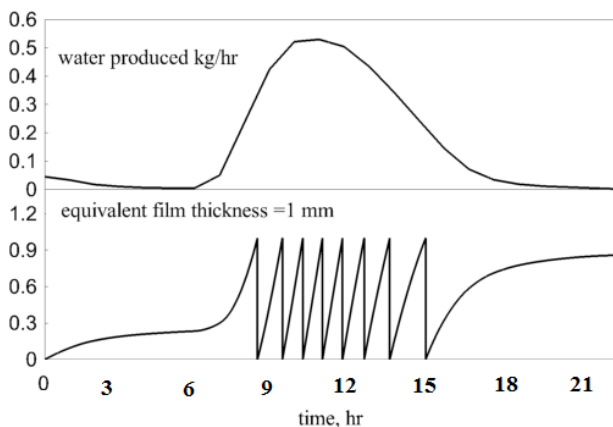


Fig. 11. Instability of a liquid film during condensation over the glass surface with an equivalent critical film thickness of 1 mm. The growth in film thickness post 15 h arises from low evaporation rates from warm water when the solar flux of late evening has effectively become zero.

inner and outer glass temperatures are greatly impacted, showing a definite increase in glass temperature relative to a zero water film thickness. The effect on the maximum temperature attained in water is also monotonic. The increase in effective sink temperature of mainly glass, lowers the evaporation rate of water, increasing the temperature of water in the basin. To an extent, the increase in both the source and sink temperature nullifies any degradation in pure water production and nearly constant water productivity is obtained.

4. Effect of water depth and salinity on performance of doubly inclined solar still

Experiments were conducted for various water layer thicknesses, namely, 10, 30, and 50 mm. The quantity of greatest importance is the water produced by the solar still (Fig. 12). Specifically, water produced on an hourly basis and the cumulative water produced per day are of interest. These measurements have been carried out over a five-day

Table 3

Effect of water film thickness δ (mm) on maximum temperatures attained in the solar still and peak water production. The absorption coefficient of commercial grade glass is 9.6 m^{-1} . When a condensate layer forms on the glass sheet, absorptivity of the glass-water combination is utilized in computations

Glass sheet mm	Peak water production, $\text{kg}/\text{m}^2\text{-day}$		Inner glass temperature, $^{\circ}\text{C}$		Outer glass temperature, $^{\circ}\text{C}$		Water temperature, $^{\circ}\text{C}$	
	$\delta=0$	$\delta=1$	$\delta=0$	$\delta=1$	$\delta=0$	$\delta=1$	$\delta=0$	$\delta=1$
5	3.96	3.96	66.5	67.7	63.7	63.9	75.7	76.6
1	3.99	3.99	63.2	64.4	62.7	62.9	73.5	74.3

Glass sheet thickness, mm	1 ($\delta=0$)	2 ($\delta=1$)	5 ($\delta=0$)	6 ($\delta=1$)
α absorptivity	0.00957	0.01907	0.047	0.05761

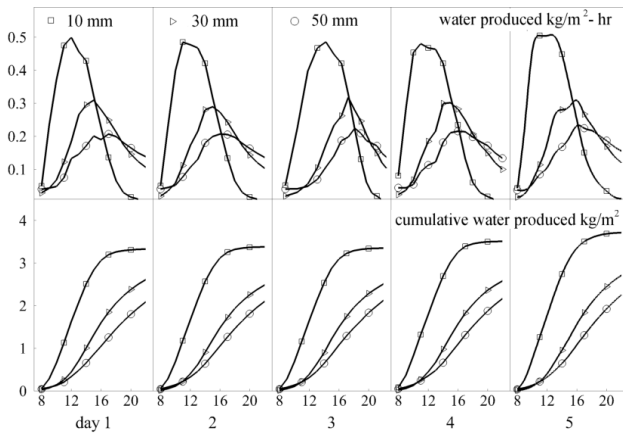


Fig. 12. Effect of water layer thickness. Variation of measured water production rate from the salt water solar still. Top row shows the water produced in $\text{kg}/\text{m}^2\text{-h}$ and bottom row shows the cumulative water produced in kg/m^2 .

period. Data was collected for the three solar stills with water depths of 10, 30, and 50 mm. Water production with the smallest water depth was seen to be the highest. It corresponds with the highest water temperature attained in the 10 mm water still. The water production rate follows the peak temperature attained, rising sharply for the basin with the smallest depth. Water production continues for a longer time period for a basin with greater water depth. In fact, for a water layer of 50 mm, water production continues even after the solar flux has become zero, mainly because the water temperature remains high enough. The cumulative water production, however, shows that a longer duration of water recovery is not adequate to compensate for high volumes of early evaporation in a basin with small water depth. Thus, the solar still with 10 mm water layer thickness is seen to demonstrate the highest rate of water production. For 30 and 50 mm solar stills, differences are not substantial since peak water temperatures attained are not distinct.

Thermal resistances that are likely to affect heat transfer across the solar still are those arising from the body of water, air gap, and the glass sheet thickness. Interfacial resistances at the water-basin boundary, water-air, and air-

glass are also important. Since the water body is, mostly, at a uniform temperature, this resistance is not significant. Similarly, the glass sheet thickness is constant for the experiments discussed and uniformly affects the device performance. For a given height of the still, an increase in water layer thickness decreases the air gap and lowers this resistance. In principle, this can have a favorable effect on water production. This expectation is not supported by the measurements carried out. Experimental data of temperature distribution as well as water production do not reveal any pronounced role of air gap. Apart from solar flux, the data is strongly influenced by the water layer height, with the influence of changes in air gap being inconsequential. It is expected that glass sheet thickness and ambient temperature will play stronger roles and will be examined in the future work.

The data of Fig. 12 is re-plotted using the mathematical model and is shown in Fig. 13. The three water depths of 10, 30, and 50 mm are again considered. Hourly as well as cumulative water produced are presented. The 10 mm layer solar still shows the best performance in terms of water produced. The peak water production rate as well as the daily water produced show a good match with the experiments of Fig. 12. The model shows a clear degradation in water production when the layer height is increased from 30 to 50 mm. This trend arises from a sharp reduction in the peak water temperature for a 50 mm water layer, where the reduction is jointly affected by a slow temperature rise and fall in the solar flux later in the afternoon hours.

4.1. Reduction in water production with salt concentration

The reduction in the production of fresh water with salt concentration can be related to the changes in the thermo-physical properties of the solution contained in the solar still. These properties include density, specific heat, thermal conductivity, viscosity, absorptivity, latent heat of vaporization and vapor pressure. Using the mathematical model, sensitivity of water production with each of these parameters was systematically investigated. Despite large changes in density, water production was not particularly sensitive to it. The single most important factor causing a reduction in water production was identified as the change in vapor pressure with salt concentration [Eqs. (11) and

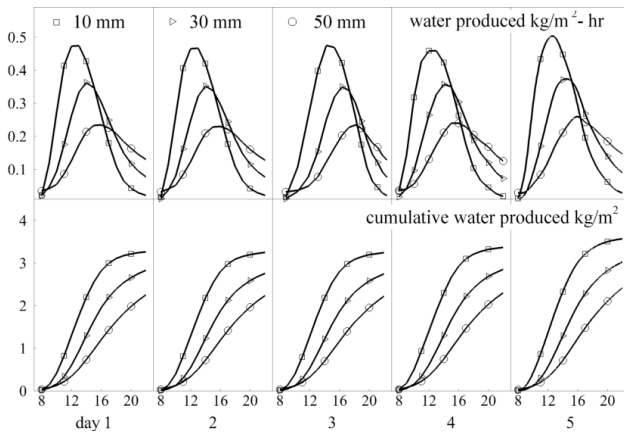


Fig. 13. Effect of depth of water on water productivity for water depths 10, 30 and 50 mm in the mathematical model.

(12)]. The extent of sensitivity to vapor pressure matched water production in the model as well as experiments.

The changes in solar still performance with temperature and salt concentration can be explained primarily in terms of changes in vapor pressure. This dependence is contained in Eqs.(10)–(12) and is plotted in Fig. 14. With increase in water temperature, vapor pressure increases monotonically, reaching atmospheric pressure at 100°C. A higher vapor pressure with temperature reveals an increasing tendency for evaporation and is a favorable trend. Thus, high water temperature, as realized in shallow water stills will increase water production. Vapor pressure diminishes in the presence of salt and is seen in Fig. 14. As per Raoult's law, the reduction is in inverse proportion as the salt concentration. These trends explain the lowering of water production with salt concentration.

It is appropriate to see if the lowering of vapor pressure by salt concentration can be compensated by an increase in temperature. The latter is enabled when water depth in the solar still is kept low. It suggests that solar stills with salt solution should operate at low water depths so as to increase temperature and compensate for a loss of vapor pressure.

Fig. 15 shows the variation of water production with respect to water depth for varying salt (NaCl) concentration. As the water depth increases, water output decreases, as expected. For a given depth, water production decreases with increasing salt concentration. The graphs are non-overlapping and the possibility of accounting for salt concentration in the water output is not visible.

To examine if the reduction in water production arises entirely from a loss of vapor pressure, the data of Fig. 15 was generated from the model by keeping vapor pressure independent of molarity while making other properties such as density and specific heat, functions of salt concentration. The data practically overlapped the zero molarity result of Fig. 15, confirming the importance of vapor pressure as central to the still performance.

Additionally, Fig. 15 shows a distinct trend in that the water output increases rapidly for small depth and flattens subsequently. The discontinuity in slope is prominent at higher salt concentrations. This result can be attributed to the relative magnitudes of latent heat and sensible heat of

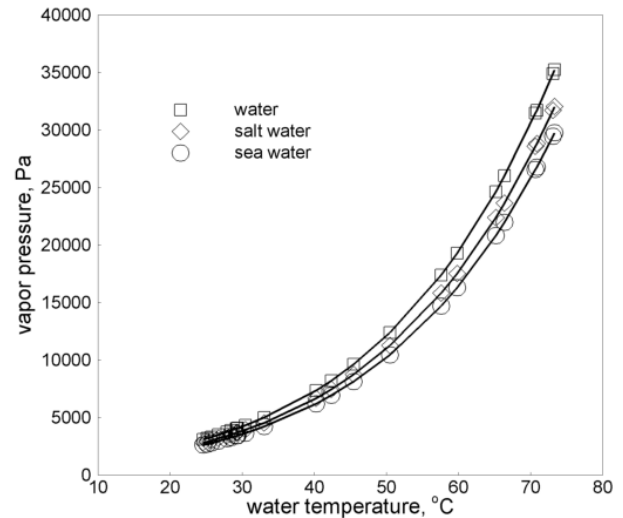


Fig. 14. Effect of water temperature and salt concentration on vapor pressure.

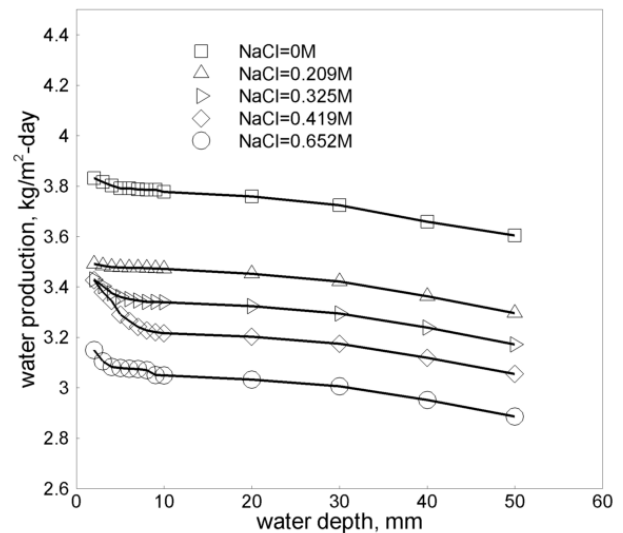


Fig. 15. Variation of water production for water and salt water with different salinity at different water depths; symbol M represents the molarity of the solution. Pure water is 0 M, 0.419 M is 24 g of NaCl in 1 L of water and 0.625 M represents an equivalent composition of seawater.

the solution. For small depths, the former is expected to be a significant fraction, diminishing in importance with an increasing depth of the water layer. A sensitivity analysis involving latent heat of evaporation as a parameter showed the change in slope to fade away for smaller latent heats. Increasing salt concentration raises density and specific heat, and hence the sensible heat fraction, clearly demarcating the still performance at small and large water depths.

Fig. 16 shows the variation of peak water temperature as a function of water depth and salinity. As water depth increases the peak water temperature decreases. Similarly, with increase in salt concentration from 0 to 36 g of salt

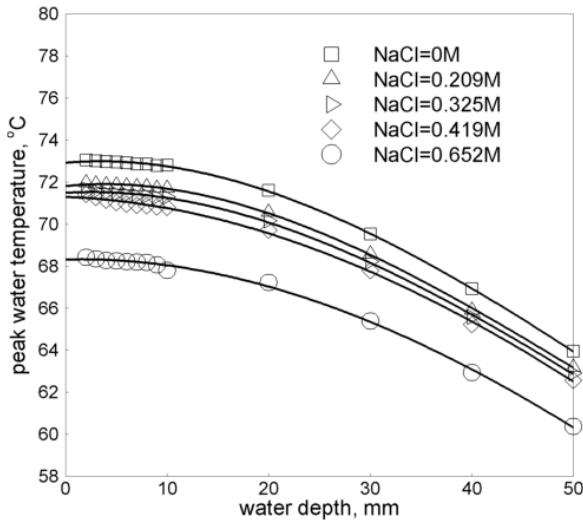


Fig. 16. Variation of peak water temperature for water and salt water with varying salinity at different water depths.

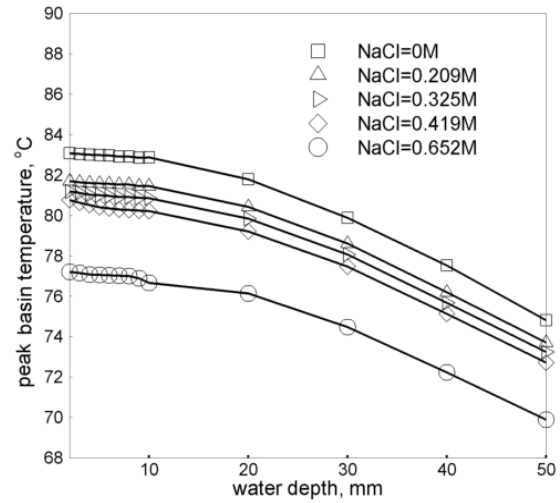


Fig. 17. Variation of peak basin temperature for water and salt water with different salinity at different water depths.

(0–0.652 M) per 1 L of water, the peak water temperature decreases. The two regimes of low and high water depths seen in Fig. 15 is again reproduced. The reduction in peak water temperature with depth and salt content arise from the increase in thermal capacity of water. Apart from a lowering of vapor pressure with molarity, the reduction in peak water temperature contributes additionally to a diminished water production seen in Fig. 15. Fig. 17 shows the variation of peak basin temperature as a function of water depth and salinity.

4.2. Peak basin temperature

Fig. 17 shows the variation of peak basin temperature as a function of water depth and salinity.

The basin temperature data follows the trend seen in the water temperature, except that it is higher. The difference between the two is a measure of loss of performance of the solar still. Basin-water temperature difference can be lowered by heat transfer enhancement features such as fins and forced convection.

An independent measure of the solar still performance is the time taken by water to reach peak temperature on a given day. A delay on this front lowers the average water temperature, thus lowering water productivity. Fig.18 shows the time required to reach the peak water temperature for pure water, salt water and seawater inside the solar still for various water depths. It is seen that time required is practically constant for pure as well as saline solutions. The result arises from the fact temperature rise is strongly linked with the temporal variation of solar flux, both reaching a maximum near mid-day, and cooling off entirely at night time. This trend is reproduced in simulations as well as experiments.

5. Density measurement

Density of the condensate has been measured over a five-day period. Here, 40 ml water was collected periodically from underneath the glass surface and weighed using

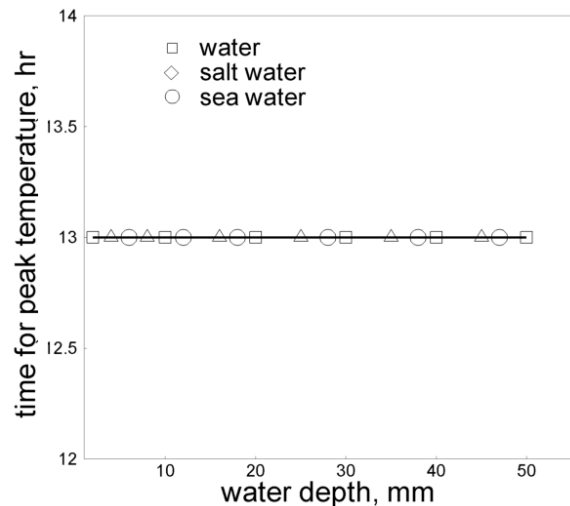


Fig. 18. Time required reaching the peak water temperature for pure water, salt water and seawater inside the solar still.

a precision balance. The purpose of this measurement is to examine the possibility of salt being transferred to the condensate and the effectiveness of the transport processes in the solar still. Density of randomly collected water samples from a water distillation plant are included (labeled ‘distillate’). Water densities are reported at 30°C. From 100 samples, densities (in units of kg/m³) recorded are, 981.88 ± 1.8 for the distillate, 988.17 ± 2.7 for pure water, and 1073.6 ± 2.6 for salt water. The pure water data matches that of the condensate, confirming the quality of the condensation process.

6. Water quality

Two condensate samples were extracted from under the glass cover of the solar still containing salt water. Water

quality was tested using an inductively coupled plasma mass spectrometry system (ICP-MS) for traces of a variety of elements.

In mass spectrometry, metals and several non-metals are detected at concentrations as low as one part in 10^{15} (part per quadrillion, ppq) on non-interfered low-background isotopes. This is achieved by ionizing the sample with inductively coupled plasma and then using a mass spectrometer to separate and quantify those ions.

Chemical composition thus obtained is listed in Table 4 along with limits desirable in potable water. The data shows the chemical components are small and within permissible limits. Most elements are below the detection limit in the distillate. Consistent measurements were recorded with samples 1 and 2 confirming the repeatability of compositional analysis.

7. Discussion: enhancement in still performance

Experiments show that the basic solar still has a water output of 2 to 4 kg/m²/d. The issue of increasing water productivity is hence of importance. The data obtained in the present study points towards certain measures that can be adopted in this context. These are listed below.

- Water output scales closely with the solar flux; hence increasing solar flux using concentrators will improve water output [39,40].
- Water production rate diminishes to zero at the end of the day. The productivity can be extended beyond daylight hours using energy storage materials. Placement of tubes containing phase change material (PCM) is recommended within the solar still [41,42].
- A hydrophobic coating over the glass surface will encourage dropwise condensation and drain water

away. Thus, thermal resistance at the glass cover can be reduced [37]. Other methods of increasing condensation surface area will be beneficial [43].

- The basin temperature and water temperature are significantly different, the basin being at a higher temperature. Thermal resistance in the basin can be reduced by flowing water, using, for example, a thermosyphon arrangement [44].
- A substantial part of the day goes towards warming up water. The transient duration can be reduced by lowering the water depth.

8. Conclusions

The productivity and performance of doubly inclined solar still has been studied over a period of five consecutive clear days. The working media are pure water, salt water and equivalent seawater. Measurements of temperature distribution and water production are compared against a mathematical model. The following conclusions have been arrived at in the present study.

- Hourly and daily water production rates decrease with increase in salt concentration. This trend is mainly because of the lowering of the vapor pressure of a solution. These trends as well as others in terms of temperature profiles are well-reproduced in the mathematical model. Temperatures follow the solar flux closely, which in turn determines the water production rate.
- Lower water depths increase water temperature and increase condensate output. The relative magnitudes of sensible and latent heats introduce distinct regimes in water productivity data.

Table 4

Water quality parameter testing using ICPMS method. The following abbreviations are used: BDL – Below Detection Limit; NTU – Nephelometric Turbidity Unit; The applicable detection Limits are Pb 0.0001 mg/l, Cu 0.0001 mg/l, Cr 0.0005 mg/l, Fe 0.0001 mg/l, Cd 0.0004 mg/l, As 0.0001 mg/l, Zn 0.0005 mg/l

Parameters	Permissible limit	Maximum limit	Sample 1	Sample 2
pH	6.5 to 8.5	No relaxation	7.2	7.3
TDS (mg/l)	500	2000	13.3	5.3
Hardness (as CaCO ₃) (mg/l)	300	600	10	20
Alkalinity (as CaCO ₃) (mg/l)	200	600	20	10
Nitrate (mg/l)	50	No relaxation	0.256	0.349
Sulfate (mg/l)	200	400	0.014	0.016
Chloride (mg/l)	250	1000	5.0	5.0
Turbidity (NTU)	5	10	0.002	0.001
Arsenic (mg/l)	0.01	No relaxation	BDL	BDL
Copper (mg/l)	0.05	1.5	0.022	0.059
Cadmium (mg/l)	0.01	No relaxation	BDL	BDL
Chromium (mg/l)	0.05	No relaxation	BDL	BDL
Lead (mg/l)	0.05	No relaxation	BDL	BDL
Iron (mg/l)	0.3	1	0.031	0.039
Zinc (mg/l)	5	15	0.375	0.233

- Experimental data matches the mathematical model when heated water temperature in the still is given as an input, instead of the solar flux.
- The presence of a condensate film on the inner side of the glass cover whose limiting thickness is experimentally determined along with periodic drainage is considered in the model. Including corrections for thermal conductivity and the absorption coefficient, it is seen that water and basin temperatures visibly increase but water production is barely affected.
- The quality of condensate sampled over the five-day period matches that of distilled water in terms of density. Chemical analysis of the condensate does not reveal any trace of the solute and other dissolved minerals.
- Condensation patterns on the glass sheet and their temporal characteristics depend on surface hydrophobicity but not on the composition of the solution in the solar still.

q_b	— Rate of heat transfer from basin liner to ambient (W/m^2)
U_t, U_b	— Overall top and bottom heat loss coefficient ($W/m^2\ ^\circ C$)
T_a	— Ambient temperature ($^\circ C$)
T_b	— Basin temperature ($^\circ C$)
T_{si}, T_{so}	— Inner and outer surface glass cover temperatures ($^\circ C$)
T_{sky}	— Temperature of sky ($^\circ C$)
T_w	— Water temperature ($^\circ C$)
α, ε	— Absorptivity, emissivity
σ	— Stefan Boltzmann constant
σ_s	— Surface tension of water (N/m)
δ_{max}	— Film thickness (m)
ρ, ρ_v	— Density of water and water vapor (kg/m^3)
μ	— Viscosity of water ($kg/m\cdot s$)
ΔT	— Temperature difference (K)

Funding: This research did not receive any specific grant from funding agencies in the public, commercial, or not-for-profit sectors.

Symbols

$h_{c,g-a}$	— Convective heat transfer coefficient from glass cover to ambient ($W/m^2\cdot K$)
$h_{r,g-a}$	— Radiative heat transfer coefficient from glass cover to ambient ($W/m^2\cdot K$)
$h_{t,g-a}$	— Total (convective & radiative) heat transfer coefficient from glass cover to ambient ($W/m^2\cdot K$)
$h_{c,w-g}$	— Convective heat transfer coefficient from water to glass cover ($W/m^2\cdot K$)
$h_{e,w-g}$	— Evaporative heat transfer coefficient from water to glass cover ($W/m^2\cdot K$)
$h_{r,w-g}$	— Radiative heat transfer coefficient from water to glass cover ($W/m^2\cdot K$)
I_t	— Intensity of solar radiation over the inclined surface of the solar still (W/m^2)
K, K_g	— Thermal conductivity of water and glass cover ($W/m\cdot K$)
C_w	— Specific heat of water in solar still ($J/kg\ ^\circ C$)
h_{fg}	— Latent heat of vaporization (J/kg)
L, L_g	— Length of the condensing surface and thickness of insulation glass cover (m)
M_{ew}	— Daily output from solar still ($kg/m^2\ day$)
P_{gi}	— Partial vapour pressure at inner surface glass temperature (N/m^2)
P_w	— Partial vapour pressure at water temperature (N/m^2)
$q_{c,w-g}$	— Rate of convective heat transfer from water to glass cover (W/m^2)
$q_{e,w-g}$	— Rate of evaporative heat transfer from water to glass cover (W/m^2)
$q_{r,w-g}$	— Rate of radiative heat transfer from water to glass cover (W/m^2)
$q_{r,g-a}$	— Rate of radiative heat transfer from glass cover to ambient (W/m^2)
$q_{c,g-a}$	— Rate of convective heat transfer from glass cover to ambient (W/m^2)
q_w	— Rate of convective heat transfer from basin liner to water (W/m^2)

References

- T.B. Nguyen, Factors affecting the yield of solar distillation systems and measures to improve productivity, *Desal. Water Treat.*, 68 (2017) 91–98.
- M. Boubekri, A. Chaker, A. Cheknane, Modeling and simulation of the continuous production of an improved solar still coupled with a photovoltaic/thermal solar water heater system, *Desalination*, 331 (2013) 6–15.
- H. Taghvaei, H. Taghvaei, K. Jafarpur, M.K. Estahbanati, M. Feilizadeh, M. Feilizadeh, A.S. Ardekani, A thorough investigation of the effects of water depth on the performance of active solar stills, *Desalination*, 347 (2014) 77–85.
- A. Ahsan, M. Imteaz, U. Thomas, M. Azmi, A. Rahman, N.N. Daud, Parameters affecting the performance of a low cost solar still, *Appl. Energy*, 114 (2014) 924–930.
- R. Dev, S.A. Abdul-Wahab, G. Tiwari, Performance study of the inverted absorber solar still with water depth and total dissolved solid, *Appl. Energy*, 88 (2011) 252–264.
- M. Rajamanickam, A. Ragupathy, Influence of water depth on internal heat and mass transfer in a double slope solar still, *Energy Procedia*, 14 (2012) 1701–1708.
- H.S. Aybar, H. Assefi, Simulation of a solar still to investigate water depth and glass angle, *Desal. Water Treat.*, 7 (2009) 35–40.
- R. Bakari, R.J. Minja, K.N. Njau, Effect of glass thickness on performance of flat plate solar collectors for fruits drying, *Energy*, 2014 (2014).
- H.N. Panchal, P. Shah, Effect of Varying glass cover thickness on performance of solar still: in a winter climate conditions, *IJRER*, 1 (2012) 212–223.
- A.J.N. Khalifa, On the effect of cover tilt angle of the simple solar still on its productivity in different seasons and latitudes, *Energy Convers. Manage.*, 52 (2011) 431–436.
- A.J.N. Khalifa, A.M. Hamood, Effect of insulation thickness on the productivity of basin type solar stills: An experimental verification under local climate, *Energy Convers. Manage.*, 50 (2009) 2457–2461.
- M. Castillo-Téllez, I. Pilatowsky-Figueroa, Á. Sánchez-Juárez, J.L. Fernández-Zayas, Experimental study on the air velocity effect on the efficiency and fresh water production in a forced convective double slope solar still, *Appl. Therm. Eng.*, 75 (2015) 1192–1200.
- E. Rubio, M.A. Porta, J.L. Fernandez, Cavity geometry influence on mass flow rate for single and double slope solar stills, *Appl. Therm. Eng.*, 20 (2000) 1105–1111.

- [14] M. Feilizadeh, M.K. Estahbanati, A. Ahsan, K. Jafarpur, A. Mersaghian, Effects of water and basin depths in single basin solar stills: An experimental and theoretical study, *Energy Convers. Manage.*, 122 (2016) 174–181.
- [15] A. Madhlopa, Modelling radiative heat transfer inside a basin type solar still, *Appl. Therm. Eng.*, 73 (2014) 707–711.
- [16] N. Rahbar, J. Esfahani, Productivity estimation of a single-slope solar still: Theoretical and numerical analysis, *Energy*, 49 (2013) 289–297.
- [17] J. Xiong, G. Xie, H. Zheng, Experimental and numerical study on a new multi-effect solar still with enhanced condensation surface, *Energy Convers. Manage.*, 73 (2013) 176–185.
- [18] G. Tiwari, S. Shukla, I. Singh, Computer modeling of passive/active solar stills by using inner glass temperature, *Desalination*, 154 (2003) 171–185.
- [19] H.N. Panchala, S. Patelb, Comparative analysis of indoor and outdoor tests on solar still.
- [20] K. Sampathkumar, T. Arjunan, P. Pitchandi, P. Senthilkumar, Active solar distillation—a detailed review, *Renew. Sust. Energy Rev.*, 14 (2010) 1503–1526.
- [21] J. Mahdi, B. Smith, A. Sharif, An experimental wick-type solar still system: design and construction, *Desalination*, 267 (2011) 233–238.
- [22] K.S. Spiegler, *Principles of Desalination*, Elsevier, 2012.
- [23] S. Rai, D. Dutt, G. Tiwari, Some experimental studies of a single basin solar still, *Energy Convers. Manage.*, 30 (1990) 149–153.
- [24] A.O. Edeoja, F. Unom, J. Edeoja, Investigation of the effect of angle of cover inclination on the yield of a single basin solar still under Makurdi climate, *Int. J. Eng. Sci.*, 2 (2013) 131–138.
- [25] L. Anjaneyulu, E.A. Kumar, R. Sankannavar, K.K. Rao, Defluoridation of drinking water and rainwater harvesting using a solar still, *Ind. Eng. Chem. Res.*, 51 (2012) 8040–8048.
- [26] T. Arunkumar, K. Vinothkumar, A. Ahsan, R. Jayaprakash, S. Kumar, Experimental study on various solar still designs, *ISRN Renew. Energy*, 2012 (2012).
- [27] S. Kumar, A. Dubey, G. Tiwari, A solar still augmented with an evacuated tube collector in forced mode, *Desalination*, 347 (2014) 15–24.
- [28] T. Elango, K.K. Murugavel, The effect of the water depth on the productivity for single and double basin double slope glass solar stills, *Desalination*, 359 (2015) 82–91.
- [29] Z. Omara, A. Kabeel, M. Younes, Enhancing the stepped solar still performance using internal and external reflectors, *Energy Convers. Manage.*, 78 (2014) 876–881.
- [30] R. Sathyamurthy, H.J. Kennady, P. Nagarajan, A. Ahsan, Factors affecting the performance of triangular pyramid solar still, *Desalination*, 344 (2014) 383–390.
- [31] M. Morad, H.A. El-Maghawry, K.I. Wasfy, Improving the double slope solar still performance by using flat-plate solar collector and cooling glass cover, *Desalination*, 373 (2015) 1–9.
- [32] H.B. Halima, N. Frikha, R.B. Slama, Numerical investigation of a simple solar still coupled to a compression heat pump, *Desalination*, 337 (2014) 60–66.
- [33] G. Xiao, X. Wang, M. Ni, F. Wang, W. Zhu, Z. Luo, K. Cen, A review on solar stills for brine desalination, *Appl. Energy*, 103 (2013) 642–652.
- [34] H. Al-Hinai, M. Al-Nassri, B. Jubran, Parametric investigation of a double-effect solar still in comparison with a single-effect solar still, *Desalination*, 150 (2002) 75–83.
- [35] G. Tiwari, A.K. Tiwari, *Solar distillation practice for water desalination systems*, Anshan Pub, 2008.
- [36] V. Sivakumar, E. Ganapathy Sundaram, MATLAB modelling and examination of the effect of heat capacity of basin and glass cover on performance of solar still by thermal models, *Int. J. Amb. Energy*, 39 (2018) 1–10.
- [37] D.J. Preston, D.L. Mafra, N. Miljkovic, J. Kong, E.N. Wang, Scalable graphene coatings for enhanced condensation heat transfer, *Nanoletters*, 15 (2015) 2902–2909.
- [38] B.S. Sikarwar, N.K. Battoo, S. Khandekar, K. Muralidhar, Drop-wise condensation underneath chemically textured surfaces: simulation and experiments, *Int. J. Heat Transfer*, 133 (2011) 021501.
- [39] C.-W. Liang, J.-S. Lin, High concentration thin profile solar concentrator utilizing toroidal confocal relay, *Solar Energy*, 122 (2015) 264–270.
- [40] R.J. Xu, X.H. Zhang, R.X. Wang, S.H. Xu, H.S. Wang, Experimental investigation of a solar collector integrated with a pulsating heat pipe and a compound parabolic concentrator, *Energy Convers. Manage.*, 148 (2017) 68–77.
- [41] M. Kenisarin, K. Mahkamov, Solar energy storage using phase change materials, *Renew. Sustain. Energy Rev.*, 11 (2007) 1913–1965.
- [42] F. Sarhaddi, F.F. Tabrizi, H.A. Zoori, S.A.H.S. Mousavi, Comparative study of two weir type cascade solar stills with and without PCM storage using energy and exergy analysis, *Energy Convers. Manage.*, 133 (2017) 97–109.
- [43] R. Bhardwaj, M. ten Kortenaar, R. Mudde, Influence of condensation surface on solar distillation, *Desalination*, 326 (2013) 37–45.
- [44] S.J. Mamouri, H.G. Derami, M. Ghiasi, M. Shafii, Z. Shiee, Experimental investigation of the effect of using thermosyphon heat pipes and vacuum glass on the performance of solar still, *Energy*, 75 (2014) 501–507.